NASA
Technical
Paper
3109

April 1991

Surface Effects on Hydrogen Permeation Through Ti-14Al-21Nb Alloy

Sankara N. Sankaran,
Ronald A. Outlaw,
and Ronald K. Clark

NASA

NASA Technical Paper 3109

1991

Surface Effects on Hydrogen Permeation Through Ti-14Al-21Nb Alloy

Sankara N. Sankaran
Analytical Services & Materials, Inc.
Hampton, Virginia

Ronald A. Outlaw and Ronald K. Clark
Langley Research Center
Hampton, Virginia

National Aeronautics and Space Administration
Office of Management
Scientific and Technical Information Division

Abstract

Hydrogen transport through Ti-14Al-21Nb (percent weight) alloy was measured using ultrahigh vacuum (UHV) permeation techniques over the temperature range from 500°C to 900°C and hydrogen pressure range from 0.25 to 10 torr. Hydrogen permeability through the alloy can be described through two different mechanisms depending on the temperature of exposure. In the range from 675°C to 900°C, the process is diffusion limited: the permeability has a weak temperature dependence, but the diffusivity has a strong temperature dependence. Below 675°C the permeation rate of hydrogen is very sensitive to surface-controlled processes such as the formation of a barrier layer from contaminants. A physical model explaining the role of surface films on the transport of hydrogen through Ti-14Al-21Nb alloy has been described.

Introduction

Titanium aluminide intermetallic alloys are being considered for use in hydrogen-fueled hypersonic vehicles because of their superior high-temperature specific strength and stiffness characteristics. Because these structures are expected to be exposed to hydrogen at temperatures ranging from cryogenic to 1000°C and to hydrogen pressures ranging from subatmospheric to over 100 atm, evaluation of the hydrogen compatibility of these alloys is very important. Ti-14Al-21Nb (percent weight) alloy is a modification of the intermetallic Ti_3Al in which Nb has been added for phase control. This alloy has received considerable attention in recent years as a candidate material for hypersonic structures. However, only a few limited studies on the hydrogen compatibility of this alloy have been reported in the literature (refs. 1 and 2). These studies have established that this alloy has a substantial solubility for hydrogen (up to 1.9 percent weight in the temperature interval from 500°C to 1050°C) and is susceptible to the formation of hydrides below 700°C.

Although the mechanisms of the interaction of hydrogen with the Ti-14Al-21Nb alloy have not been completely established, experience with pure titanium (refs. 3 and 4) and other transition metals like niobium, tantalum, and vanadium (refs. 5 and 6) shows that hydrogen causes a degradation in the mechanical properties of these materials. This degradation occurs by several mechanisms depending on the nature of the interaction. For example, because of the very low solubility of hydrogen in α-titanium at room temperature (ref. 4), brittle hydrides readily form and lead to a loss in the ductility of the metal.

Even under conditions when hydrides do not form, hydrogen in solid solution has been shown to cause a degradation in the mechanical properties of both α-titanium (ref. 7) and β-stabilized alloys of titanium (ref. 8). Thus, the severity of mechanical property degradation in titanium alloys due to hydrogen depends on the microstructural effects of hydrogen in the alloy. In general, the stability of hydrogen-induced phase changes is controlled by several factors: the pressure of hydrogen in the environment, the temperature of exposure, and the surface condition of the alloy. However, the extent of microstructural changes through the bulk of the structure depends on the transport rate of hydrogen from the environment to the interior of the metal.

The purpose of the present work was to establish the solubility and transport characteristics of hydrogen in Ti-14Al-21Nb alloy over the temperature range from 500°C to 900°C and the hydrogen pressure range from 0.25 to 10 torr. These conditions are representative of those to be encountered by regions of a hydrogen-fueled hypersonic vehicle where alloys like Ti-14Al-21Nb might be used.

Analysis

Membrane permeation is a popular technique used for the characterization of hydrogen transport through metals and alloys. The experimental procedure involves exposing one side of a thin sheet of material to gas at the desired partial pressure while maintaining the other side under ultrahigh vacuum (UHV) conditions. The simplest case of permeation is one in which surface phenomena such as sorption and desorption of gas molecules at the specimen surface and dissociation or recombination of molecules at the interfaces proceed much faster than the diffusion of atoms through the membrane. Under these conditions, the near-surface regions of the membrane are in thermodynamic equilibrium with their respective contiguous gas phase.

The time variation of hydrogen flux through the membrane (fig. 1) exhibits three distinct regimes: an

initial transient regime that begins with hydrogen exposure and continues until equilibrium conditions exist, a steady-state regime that exists during equilibrium, and a final transient regime that begins with removal of the hydrogen gas from the upstream surface and continues as the downstream pressure decays. Hydrogen transport for each of these conditions can be modeled by the solution of Fick's laws with the appropriate boundary conditions.

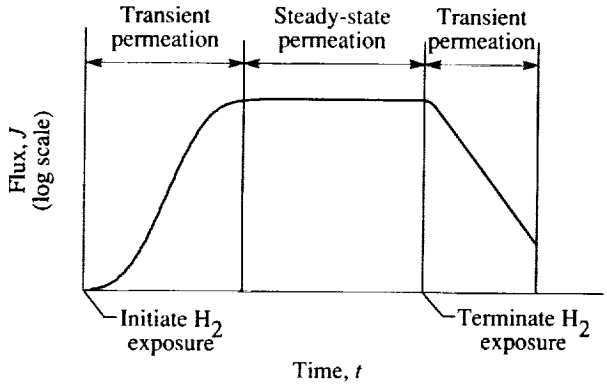

Figure 1. Time dependence of permeation through membrane.

This description of hydrogen transport is adequate for many cases. In more complex cases, phase transformations and the presence or formation of surface layers lead to the problem of permeation through laminated materials for which time-dependent solutions of the diffusion equation are more complex. However, by using the steady-state solutions developed by Perkins (ref. 9) and Ash et al. (ref. 10), permeation through a variety of systems can be analyzed as described below.

Case 1: Permeation Through a Homogeneous Membrane

A homogeneous permeation membrane is one in which surface layers are not present and in which the permeating species do not cause any phase transformations or redistribution of the existing phases in the alloy. Figure 2 is a schematic diagram representing permeation through such a membrane. In this case, the steady-state flux J_{ss} of the permeating species (hydrogen, for example) arriving at the downstream side of the membrane can be written as (refs. 9 and 11)

$$J_{ss} = \frac{-D(C_2 - C_1)}{d} \tag{1}$$

where D is the diffusivity of hydrogen in the test material, C_1 is the concentration of hydrogen in equilibrium with the gas at the upstream side, C_2

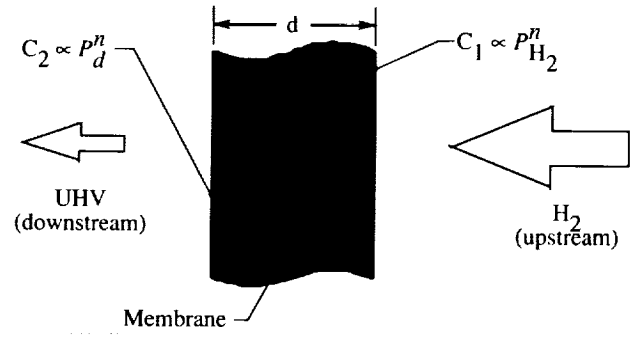

Figure 2. Schematic diagram of permeation through homogeneous membrane.

is the concentration of hydrogen in equilibrium with the gas at the downstream side, and d is the thickness of the membrane. The concentrations of hydrogen in the alloy at the near-surface regions can be related to the partial pressure of hydrogen in the gas phase as

$$C_1 = SP_{H_2}^n \tag{2a}$$

$$C_2 = SP_d^n \tag{2b}$$

where P_{H_2} is the partial pressure of hydrogen at the upstream side, P_d is the partial pressure of hydrogen at the downstream side, S is the solubility of hydrogen in the alloy, and $n = 1/2$ for the solution of diatomic gases in metals (Sievert's law) or $n = 1$ for the nondissociative solution of gases in dielectrics. Since the downstream side is always maintained under UHV conditions, it can be assumed that $C_1 >> C_2$, and thus equation (1) becomes

$$J_{ss} = \frac{DSP_{H_2}^n}{d} \tag{3a}$$

The product

$$K = DS \tag{3b}$$

is defined as the permeability of the diffusing species through the alloy. Thus, equation (3a) reduces to

$$J_{ss} = \frac{KP_{H_2}^n}{d} \tag{3c}$$

For the case of permeation at a constant temperature and upstream hydrogen pressure, the right-hand side of equation (3c) is invariant with time and, therefore, J_{ss} reaches a constant value. Thus, by experimentally measuring J_{ss}, the permeability K of a homogeneous material can be determined through equation (3c).

Although K is a material property, a complete characterization of the transport properties of a metal/alloy requires the separation of K into its components: diffusivity D and solubility S. Measurements during the nonsteady regimes of the permeation experiment can be used to determine the diffusivity. Methods for determining the diffusivity of a homogeneous material (refs. 9 and 11–13) include the time-lag method, the inflection method, and the pressure-decay method. These methods evolve from the solution of the diffusion equation for particular boundary conditions.

The time-lag method is based on the fact that the time integral of the flux becomes linear at steady state and the initial nonlinearity is equivalent to a time lag (ref. 11):

$$Q(t) = \int_0^t J\,dt \approx \frac{KP_{H_2}^n}{d}(t - \tau_L) \qquad \left(\tau_L = \frac{d^2}{6D}\right) \tag{4}$$

where $Q(t)$ is the cumulative flux of hydrogen arriving at the downstream side, τ_L is the intercept of the linear portion of the curve on the time axis, and t represents time. Diffusivity is determined from the experimentally measured value of τ_L.

The inflection method is based on determination of the time at which the nonsteady-state flux passes through an inflection point that is related to the diffusivity (ref. 12):

$$D = \frac{0.04124d^2}{J_w}\left(\frac{dJ}{dt}\right)_w \tag{5}$$

where J_w is the permeation flux at the inflection point and $(dJ/dt)_w$ is the slope of the flux at the inflection point.

The pressure-decay method is based on measurements of the decay of the downstream flux after steady-state conditions are reached and the upstream hydrogen gas source is eliminated. The decay of the flux, described by Perkins (ref. 9) and Outlaw et al. (ref. 11), becomes approximately exponential after a reasonably short time with a decay-time constant given by

$$\tau = \frac{d^2}{\pi^2 D} \tag{6}$$

Here, D is computed from the experimentally measured value of the decay constant τ.

The pressure-decay method is relatively insensitive to the fluctuations in the temperature and hydrogen pressure that may occur during the initial stages of the test since the measurements are commenced only after the attainment of steady-state conditions. This technique was therefore chosen in this work as the primary technique for the determination of diffusivity.

From a knowledge of the permeability and diffusivity of the species through a homogeneous membrane, the solubility of the permeating species in the membrane material can be calculated from equation (3b) as

$$S = \frac{K}{D} \tag{7}$$

Case 2: Permeation Through a Membrane With a Barrier Layer of Constant Thickness

Permeation through a membrane with a barrier layer is represented by the schematic diagram in figure 3. The presence of a barrier layer such as an oxide, nitride, or carbide layer on the membrane surface results in the equivalent of permeation through a laminated material in which each of the layers has its characteristic permeabilities. Since no species accumulation can occur at the interface between the barrier layer and the bulk alloy, a steady-state flux balance at the interface leads to

$$\frac{K_b\left(P_{H_2}^n - P_e^n\right)}{d_b} = \frac{KP_e^n}{d} \tag{8}$$

where K_b is the permeability of the barrier layer for hydrogen, d_b is the thickness of the barrier layer, P_e is the equilibrium pressure of hydrogen at the interface during steady-state flow, K is the permeability of hydrogen through the alloy, and d is the thickness of the membrane.

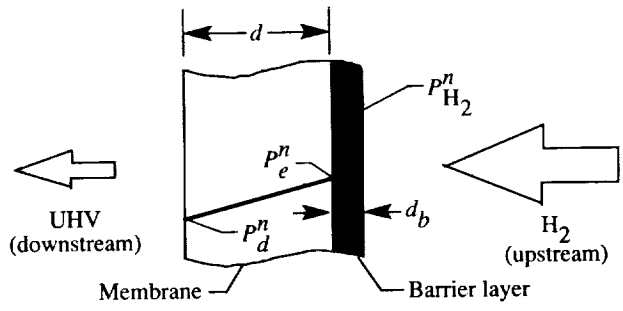

Figure 3. Schematic diagram of permeation through membrane with barrier layer.

Assuming that n has the same value for both materials, the magnitude of the flux of hydrogen

arriving at the downstream side can be determined by combining equations (3c) and (8):

$$J_{ss} = \frac{1}{\left(\frac{d_b}{d}\frac{K}{K_b}\right) + 1} \frac{K P_{H_2}^n}{d} \qquad (9)$$

When $d_b = 0$, i.e., when no barrier layer is present, this equation reduces to equation (3c). Two possibilities follow from equation (9). If $d_b/d << K_b/K$, then the term within the parentheses approaches unity and equation (9) again reduces to equation (3c), thus suggesting that the surface layer has little effect on the permeation flux. However, if $K_b/K << d_b/d$, then J_{ss} may be considerably lower than that of the pure alloy. In this case, although J_{ss} reaches a constant value at steady state, an unequivocal determination of the permeability K of the test alloy requires a knowledge of the thickness and permeability of the barrier layer.

Case 3: Permeation Through a Membrane With Growing Barrier Layer

Permeation through a membrane with a growing barrier layer is characterized by a time dependence of the permeation flux that is related to the growth of the barrier layer. Two types of processes can lead to the formation of the barrier layer: (1) deposition of a nonreacting layer on the membrane surface, and (2) formation of a reaction-product layer such as an oxide, nitride, or carbide. Since the reaction-layer formation involves consumption of the base alloy, the thickness of the alloy decreases with time. Conservation of matter at the interface and flux balance of the diffusing species at the boundary lead to

$$\frac{K_b\left(P_{H_2}^n - P_e^n\right)}{d_b(t)} = \frac{K P_e^n}{d - \alpha\, d_b(t)} \qquad (10)$$

The terms have the same meaning as in case 2 except that the barrier thickness varies with time and α is a factor to account for the consumption of the bulk alloy as the barrier increases in thickness. For a reaction-product layer, α is the ratio of the molar volume of the alloy to the molar volume of the reaction product or barrier compound (usually <1). The flux of hydrogen at the downstream side can be determined by combining equations (3c) and (10):

$$J_{ss} = \frac{1}{\left[\frac{d_b(t)}{d - \alpha\, d_b(t)}\frac{K}{K_b}\right] + 1} \frac{K P_{H_2}^n}{d - \alpha\, d_b(t)} \qquad (11)$$

For a deposited, nonreacting layer, $\alpha = 0$ and equation (11) reduces to equation (9) with d_b showing a time dependence. Again, for the surface layer to be an effective barrier,

$$\frac{K_b}{K} << \frac{d_b(t)}{d - \alpha\, d_b(t)}$$

Also, since d_b has a time dependence, the permeation flux will show a continuous decrease with exposure duration corresponding to the growth rate of the surface film. Further, if the permeation experiment is carried out on a clean membrane, the initial part of the experiment may show an apparent maximum in the permeating flux because of an insignificant effect of the barrier layer on permeation during the early stages of barrier formation.

Since J_{ss} depends on a number of factors like the permeability characteristics of the barrier layer and its growth rate, experimentally determining the permeability of the membrane material becomes very complex.

Case 4: Permeation Through a Membrane With Gas-Induced Phase Transformations

Permeation through a membrane with gas-induced phase transformations is a significant problem for titanium and its alloys in which hydrogen acts as an alloying element and stabilizes the β-phase or forms hydrides. Since these phases exist only at hydrogen pressures equal to or higher than their respective equilibrium dissociation pressures, phase transformations during hydrogen permeation are not observed at lower hydrogen pressures. For example, as shown in figure 4, if the hydrogen pressure at the upstream side reaches the equilibrium dissociation pressure for the hydride phase, thermodynamics dictates that a continuous layer of the hydride phase will form on the alloy surface exposed to the gas phase. During this stage the interface between the hydride phase and the alloy remains at the dissociation pressure of the hydride phase. Thus, the interfacial flux balance leads to the condition

$$\frac{1}{\Omega}\frac{d}{dt}(d_H) = \frac{K_H\left(P_{H_2}^n - P_{eq}^n\right)}{d_H} - \frac{K P_{eq}^n}{d - \beta d_H} \qquad (12)$$

where Ω is the volume of hydride formed for every atom of hydrogen, K_H is the permeability of hydrogen through the hydride phase, d_H is the instantaneous thickness of the hydride phase, P_{eq} is the hydrogen pressure at which both the alloy and the hydride phase are in equilibrium (dissociation pressure of the hydride), and β is the ratio of the molar volumes of the alloy and the hydride. However, at

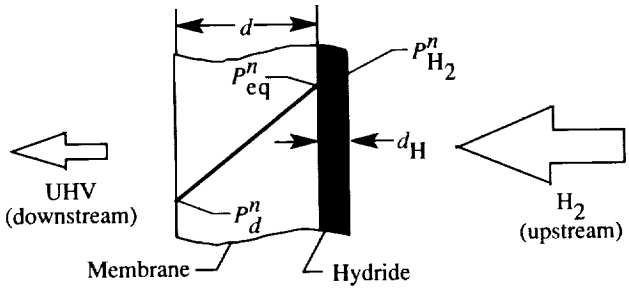

Figure 4. Schematic diagram of permeation through membrane with hydride layer.

the downstream side, the flux of hydrogen will be

$$J = \frac{KP^n_{eq}}{d - \beta d_H} \tag{13}$$

The growth of the hydride layer will continue as long as the right side of equation (12) has a positive value. The onset of the steady-state flux at the downstream side is marked by the condition $\frac{d}{dt}(d_H) = 0$, which corresponds to

$$J_{ss} = \frac{KP^n_{eq}}{d - \beta d^c_H} \tag{14}$$

where d^c_H is the equilibrium thickness of the hydride for a given exposure condition.

Equation (14) predicts that the steady-state flux has a constant value; however, the growth-rate characteristics of the hydride phase determine how soon the steady-state condition will be reached. Also, an examination of equation (13) indicates that before reaching a constant value, the flux at the downstream side will show a continuous increase over time that is related to the growth rate of the hydride phase. This behavior is in contrast to the previous case where the growth of a barrier layer was shown to lead to a continuous decrease in the hydrogen flux over time.

Experimental Procedure

The Ti-14Al-21Nb alloy used for this study was a 1.25-cm-thick rolled plate. The alloy composition provided by the vendor is listed in table I. The circular membrane test specimen (having an exposed region approximately 0.04 cm thick and a diameter of 1.6 cm) was machined with knife edges to allow assembly with metal seals between two miniflange nipples. Before assembly the membrane surfaces were mechanically polished to a 1200-grit finish, chemically cleaned to minimize oxides and residual contaminants, and heat treated under vacuum at 1100°C for

Table I. Chemical Analysis of Ti-14Al-21Nb Alloy

Element	Composition, percent weight	
	Nominal	Actual
Al	14	14.1
Nb	21	21.30
Mo		<.01
Fe		.09
V		<.01
C		.02
O		.13
N		.015
H		.0065
Zr		<.01
Ti	Balance	Balance

1.5 hr to stabilize the microstructure. In the heat-treated condition, the microstructure consisted predominantly of equiaxed α_2 grains with small amounts of an orthorhombic phase and β-phase at the grain boundaries (ref. 14).

The permeation studies were conducted in the UHV apparatus depicted in the schematic diagram in figure 5 and described previously (ref. 11). The membrane assembly was heated in a tubular furnace and was oriented such that the membrane separated the hydrogen supply side (upstream chamber) from the detection side (downstream chamber). Both sides of the membrane were initially brought to UHV conditions (lower than 10^{-8} torr).

Prior to the start of a test, the membrane was heated under vacuum to the test temperature and was maintained at that temperature for at least 1 hr before exposure to hydrogen. High-purity hydrogen, which had been liquid nitrogen cold-trapped to remove all condensibles, was then allowed to enter the upstream side of the membrane while maintaining the downstream side under UHV. The pressure of the gas at the upstream side was maintained at a constant value for each test using a pressure controller and capacitance pressure gauges. For reasons described later, experiments were conducted under two conditions: (1) stagnant conditions, where the hydrogen pressure in the upstream chamber was maintained constant at the test pressure, and (2) dynamic conditions, where dynamic flow at a constant pressure was achieved in the upstream chamber by exhausting a significant portion of the supply gas through an auxiliary valve. The tests were conducted at hydrogen pressures ranging from 0.25 to 10 torr and temperatures ranging from 500°C to 900°C .

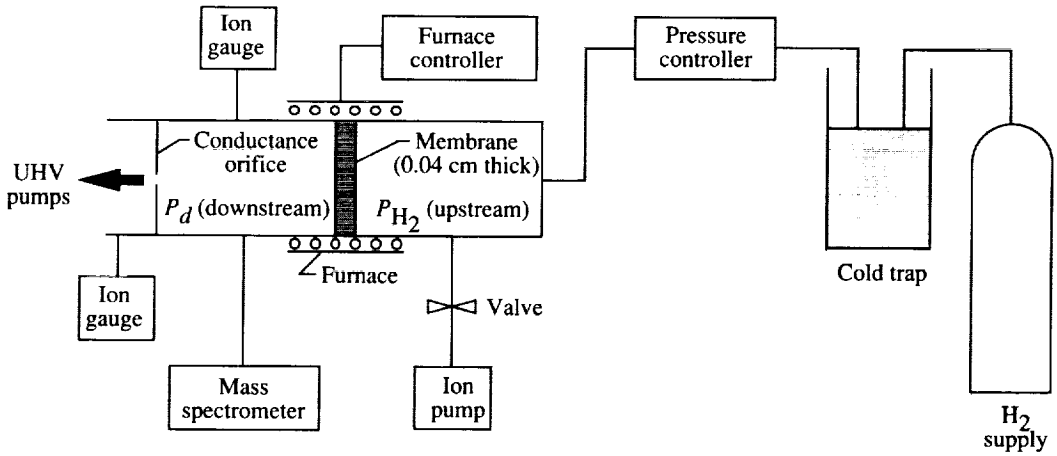

Figure 5. Schematic diagram of UHV hydrogen permeation apparatus.

The permeation of hydrogen through the membrane resulted in an increase in the downstream pressure (measured through an ion gauge) since an orifice of known conductance controlled the rate of pumping of hydrogen away from the downstream chamber. The mass flow of hydrogen through the membrane was computed from the instantaneous value of the downstream pressure using gas laws. During the test the downstream pressure was continuously monitored by feeding the output of the ion gauge through a precalibrated log amplifier to a computer and a pen recorder. In most cases the permeation experiment was continued until the steady-state conditions were established. At that stage the hydrogen gas at the upstream side was pumped away and the downstream pressure decayed to the ultimate pressure of the system.

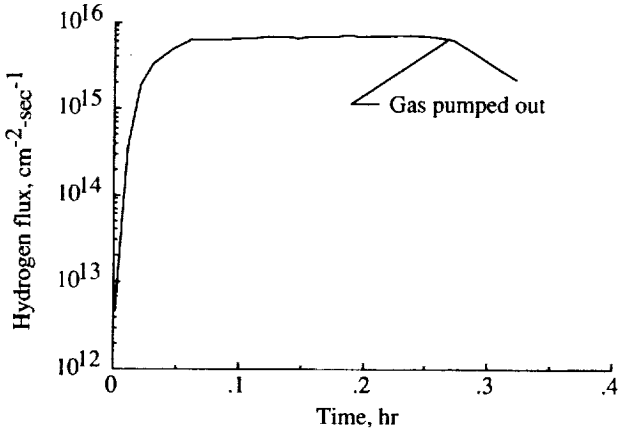

Figure 6. Hydrogen permeation flux through Ti-14Al-21Nb under stagnant conditions at 700°C and hydrogen pressure of 1 torr.

All the permeation experiments were conducted on a single membrane at temperatures increasing from 500°C to 900°C in 25°C increments. At each temperature the tests were conducted in sequence beginning at the lowest upstream pressure. A minimum of two sets of data were taken for each temperature and pressure condition to assure repeatability.

Results and Discussion

Permeation Flux

Equation (3c) indicates that for a homogeneous membrane, the steady-state permeation flux of hydrogen is constant for given conditions of temperature and pressure. This behavior is illustrated by figure 6 which shows the permeation flux of hydrogen through Ti-14Al-21Nb alloy at an exposure temperature of 700°C and a hydrogen pressure of 1 torr under stagnant conditions.

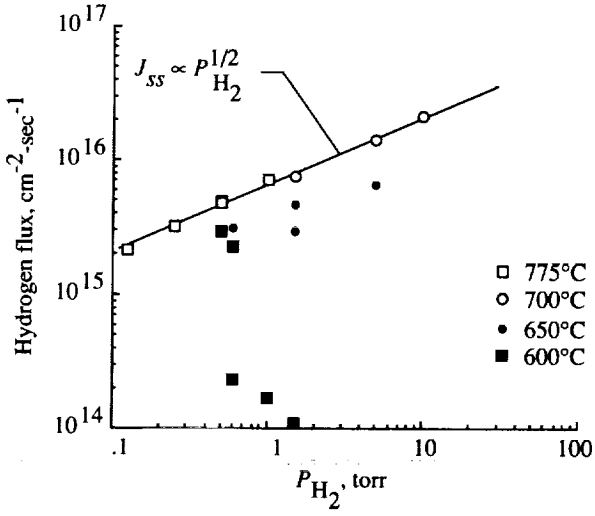

Figure 7. Hydrogen pressure dependence of permeation flux through Ti-14Al-21Nb alloy under stagnant conditions at different temperatures.

Equation (3c) also predicts that the steady-state permeation flux must exhibit a one-half-power dependence on hydrogen pressure if Sievert's law is valid. Figure 7 shows permeation flux as a function of hydrogen pressure for stagnant conditions at temperatures from 600°C to 775°C . The one-half-power pressure dependence was observed for exposure temperatures ≥700°C. At temperatures ≤650°C, the permeation flux deviated from the one-half-power pressure dependence and showed evidence of hysteresis effects that led to nonrepetitive data.

This behavior is more evident in figure 8 which shows data from two permeation runs that were conducted one after the other under identical exposure conditions (600°C and a hydrogen pressure of 1 torr) but that were separated by an intermediate vacuum anneal. The permeation flux displayed an initial increase that led to an apparent plateau, followed by a continuous decrease with time. The intermediate vacuum anneal resulted in a partial recovery of the permeation flux, but the other features remained similar to those for the initial exposure. These results show clearly that under stagnant conditions the permeation flux of hydrogen through Ti-14Al-21Nb at temperatures ≤650°C is dependent on the prior exposure history of the membrane.

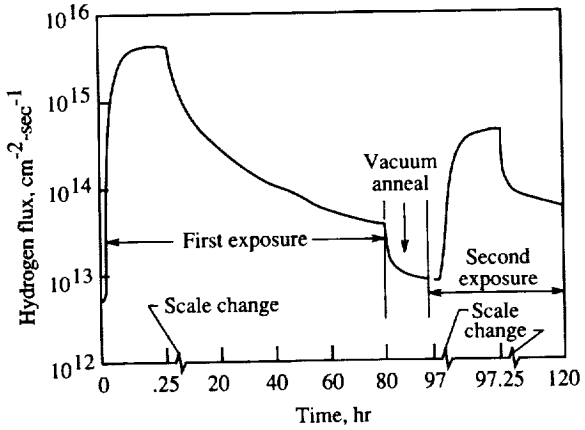

Figure 8. Effect of exposure duration and vacuum anneal on hydrogen permeation flux in Ti-14Al-21Nb alloy under stagnant conditions at 600°C and hydrogen pressure of 1 torr.

Under dynamic flow conditions the permeation flux at lower temperatures was not dependent upon the prior exposure history of the membrane. Permeation flux under dynamic conditions is contrasted with permeation flux under static conditions in figure 9 which presents data for a sequence of tests at 650°C . The first curve in the figure is for a test that was begun under stagnant conditions but was concluded under dynamic conditions (run 1). The

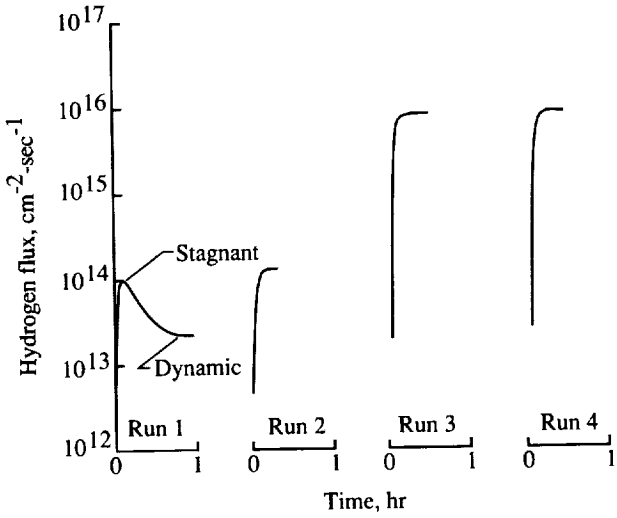

Figure 9. Effect of dynamic flow of upstream hydrogen gas on hydrogen permeation flux through Ti-14Al-21Nb alloy at 650°C and hydrogen pressure of 3 torr. (Run 1 was initiated under stagnant conditions and concluded under dynamic flow conditions; runs 2–4 were conducted under dynamic flow conditions.)

curve shows that under stagnant conditions, the permeation flux increased rapidly to a peak value and then slowly decreased with time until dynamic flow conditions were initiated and the permeation flux was stabilized. At the conclusion of the test represented by the first curve, the system was pumped to UHV conditions and hydrogen flow was initiated under dynamic conditions (run 2), thus resulting in a rapid rise in permeation flux to a stable level somewhat higher than the peak achieved during the stagnant portion of the first curve. This procedure was repeated two times (runs 3 and 4) and provided repeating values of hydrogen permeation flux that were greater than those for previous runs.

Figure 10 shows a comparison of the steady-state hydrogen permeation flux under stagnant and dynamic conditions at temperatures of 650°C and 700°C. The straight line in the figure corresponds to a half-power dependence of permeation flux on hydrogen pressure. The 700°C data for stagnant and dynamic conditions and the 650°C data for dynamic conditions correlate very well with the line. The data taken at 650°C under stagnant conditions do not correlate with the line, and the two data points at 1.5 torr are not repetitive.

Hydrogen Transport Properties of the Alloy

The data for hydrogen permeability, diffusivity, and solubility in Ti-14Al-21Nb versus temperature

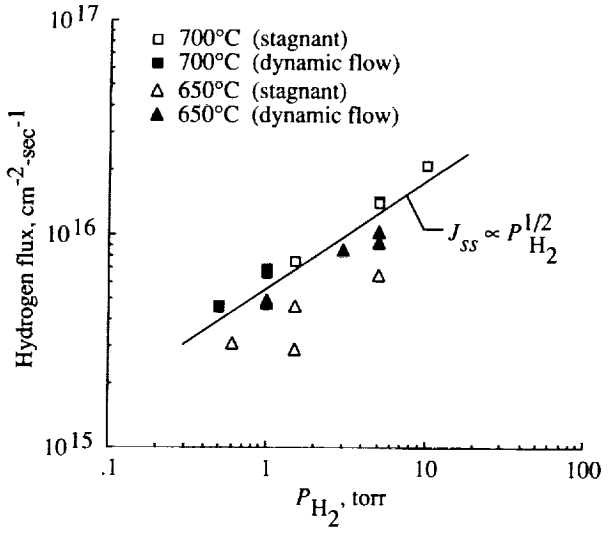

Figure 10. Variation in steady-state hydrogen permeation flux through Ti-14Al-21Nb with pressure at 650°C and 700°C under stagnant and dynamic flow conditions.

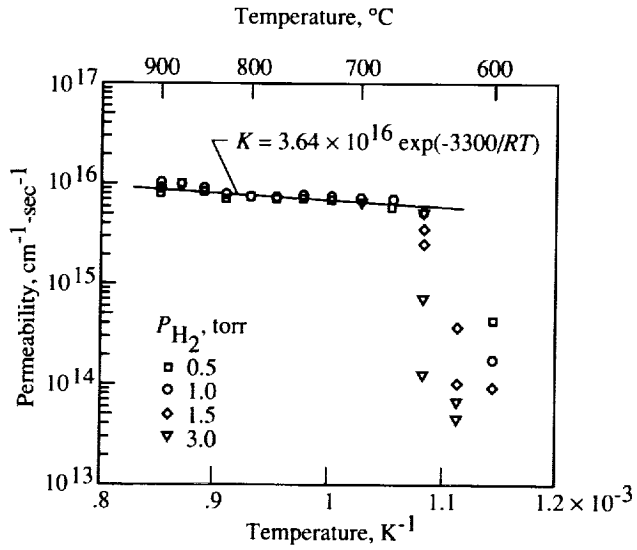

Figure 11. Permeability of hydrogen in Ti-14Al-21Nb alloy.

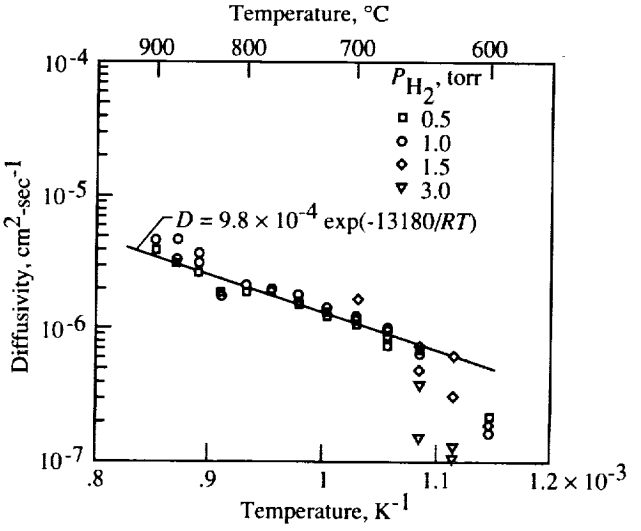

Figure 12. Diffusivity of hydrogen in Ti-14Al-21Nb alloy.

fall into two distinct temperature ranges: data for temperatures $\geq$675°C and data for temperatures $\leq$650°C. The hydrogen permeability K calculated from the measured steady-state flux, and using equation (3c) with $n = 1/2$, is summarized in figure 11. In the high-temperature range, the data are repeatable and independent of the upstream hydrogen pressure, as predicted for a homogeneous membrane. In this temperature range the permeability can be represented by an Arrhenius fit of the data:

$$K = 3.64 \times 10^{16} \exp\left(\frac{-3300\,\text{cal/mol}}{RT}\right) \text{cm}^{-1}\text{-sec}^{-1} \quad (15)$$

where R is the universal gas constant (in cal/mol/K) and T is the temperature (in K). In the low-temperature range, the calculated permeability values are lower than expected and reflect the scatter that was observed in the measured permeation flux.

Figure 12 presents data for the diffusivity of hydrogen in Ti-14Al-21Nb alloy calculated using equation (6). Again, the two temperature ranges are evident in the data. In the temperature range from 675°C to 900°C, the temperature dependence of the diffusivity is described by an Arrhenius fit of the data:

$$D = 9.8 \times 10^{-4} \exp\left(\frac{-13\,180\,\text{cal/mol}}{RT}\right) \text{cm}^2\text{-sec}^{-1} \quad (16)$$

An important feature of the diffusivity is that it has a significantly higher activation energy than the permeability.

Figure 13 presents the solubility data that were calculated from the permeability and diffusivity values using equation (7). Again, the temperature dependence of this property over the range from 675°C to 900°C can be described by an Arrhenius fit of the data:

$$S = 4.0 \times 10^{19} \exp\left(\frac{9700\,\text{cal/mol}}{RT}\right) \text{cm}^{-3} \quad (17)$$

Since the solubility data were inferred from the permeability and diffusivity values, it follows from equations (15) and (16) that solubility has a positive slope in the Arrhenius plot, thus indicating a negative enthalpy for the dissolution of hydrogen in the alloy;

i.e., solubility decreases as the temperature increases. This behavior has been noted for metals like titanium and zirconium (ref. 15).

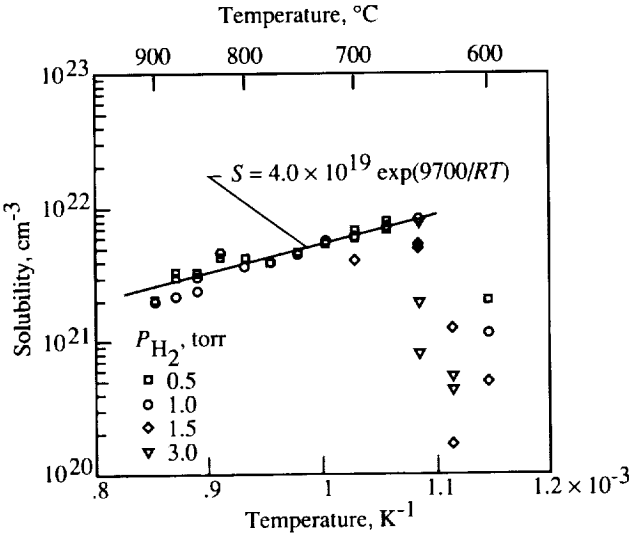

Figure 13. Solubility of hydrogen in Ti-14Al-21Nb alloy.

For a membrane of constant thickness, equation (3b) states that permeability is the product of diffusivity and solubility. Therefore, at very low pressures where the solubility S is a constant (Henry's law regime), the permeability K must be independent of the upstream hydrogen pressure. Also, since K is a characteristic property of a given phase of a material, it can be assumed from the absence of a significant variation in the permeability data as a function of hydrogen pressure over the temperature range from 675°C to 900°C (fig. 11) that no phase transitions have been induced by hydrogen over the pressures used in this temperature range. Thus, equations (15)–(17) describe the transport properties of hydrogen in the α_2-phase (the predominant phase) of the alloy.

Permeation Characteristics in the Low-Temperature Range

For temperatures ≤650°C, the dependence of the permeation flux on the exposure history, and the deviation of the permeation flux from the expected pressure dependence (eq. (3a)), indicates that the process is being limited by a different rate-controlling mechanism. A few possibilities are as follows:

1. Formation of hydrogen-induced phases on the alloy surface, such as a hydride.
2. Native films such as oxides present on the alloy surface.
3. Formation of barrier layers on the alloy surface by impurities in hydrogen.

Before attempting to decide which of these possibilities is most likely to occur, the implications and consequences of each of these processes on the permeation of hydrogen through the alloy will be explored.

Hydrogen forms a hydride phase in titanium through an eutectoid transformation (ref. 3). Under these conditions, the flux of hydrogen received at the downstream side is governed by equation (13). The attainment of the steady-state condition, in this case, is contingent upon the hydride phase reaching its ultimate thickness (d_H^c), which is a function of the upstream pressure. When the permeation process is driven by hydride formation, the growth-rate characteristics of the hydride phase will control the permeation flux at the downstream. Since both β and d_H in equation (13) are positive quantities, the permeation flux will increase with time until steady state is reached. At steady state the permeation flux will be given by equation (14). Since the low-temperature data presented in figure 8 do not reflect this trend, it is unlikely that the results for temperatures ≤650°C can be explained on the basis of hydride formation.

Because of their high reactivity with atmospheric gases, titanium and its alloys readily form surface oxides or nitrides. Equation (9) shows that the permeation flux should still reach a constant, but lower, value at the steady-state condition if native films act as a barrier layer. Several studies (refs. 16–20) have confirmed the inhibiting nature of the surface films on hydrogen permeation through titanium, particularly at temperatures below 600°C. In order to determine the nature of the interaction of hydrogen with the metal in the presence of surface oxide films, the pressure dependence of the permeation flux has been used as the controlling parameter (ref. 21). If the surface films restrict the reaction of hydrogen with the metal, the permeation flux will have a first-power dependence on the hydrogen pressure, as confirmed by a number of hydrogen permeation studies below 600°C on preoxidized and prenitrified samples of titanium (ref. 16). In the present case the dependence of the permeation flux on exposure duration and history (fig. 8) suggests that the native films cannot explain the observed results for the Ti-14Al-21Nb alloy.

As described through equation (11), the continuous decrease in the permeation rate of hydrogen through the membrane as a function of the exposure duration indicates that the process is limited by a barrier layer that grows in thickness with prolonged exposure. The dynamic nature of the process

suggests that the barrier-layer growth is triggered by the hydrogen gas itself because of impurities. Retardation in the permeation rate of hydrogen through titanium due to impurities in the gas has also been noted by other investigators (refs. 18 and 22).

Permeation Model

If the hydrogen gas at the upstream side of the membrane is contaminated with small amounts of oxygen, water vapor, or other species like CO, the high reactivity of titanium with these species will lead to the formation of a surface layer. A comparison of equations (9) and (11) indicates that the effectiveness of the surface layer as a barrier to hydrogen transport depends on its thickness. Since titanium and its alloys also have the ability to dissolve species such as C and O, the thickness of the surface layer will depend on the mass balance between two competing mechanisms: layer formation k_1 and layer dissolution k_2 depicted in the schematic diagram in figure 14.

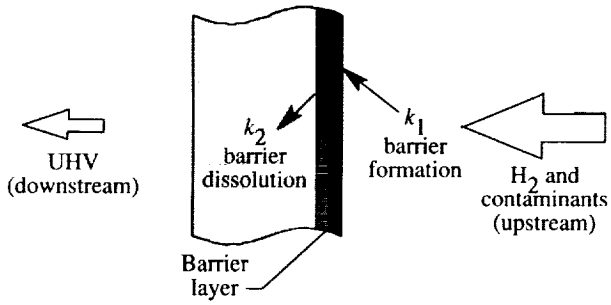

Figure 14. Model for hydrogen transport through membrane with barrier layer.

Since the surface-layer formation due to the impurities occurs under very low partial pressures of the reactant species, the rate of growth of the layer is likely to be limited by the rate of impingement of the molecules. The kinetics of this process can be written through a slight modification of the Hertz-Knudsen-Langmuir equation (ref. 23) as

$$j_x = s(1-\theta)\frac{P_x}{(2\pi M_x RT)^{1/2}} \qquad (18)$$

where j_x is the flux of impinging impurity molecules, P_x is the partial pressure of the species in the chamber, M_x is the molecular weight of the species, R is the gas constant, T is the absolute temperature, s is the sticking coefficient, and θ is the coefficient of coverage of the layer (oxide, nitride, or carbide depending on the impinging species) on the alloy surface.

For $s = 1$ and a small existing coverage on the alloy surface (i.e., θ is small), equation (18) predicts that the growth rate of the barrier layer is directly proportional to P_x and inversely proportional to T. Since the impurities are assumed to be contained in the incoming hydrogen gas, it follows that P_x will be proportional to the upstream hydrogen pressure. In other words, the barrier-layer growth rate, and therefore its effectiveness, will increase with increase in upstream hydrogen pressures and decrease with high temperatures of exposure. At low temperatures where barrier-layer formation is faster than barrier-layer dissolution, the permeation flux of hydrogen will decrease with an increase in the partial pressure of hydrogen and with prolonged exposure. Thus, the low-temperature data of figures 7 and 8 are rationalized.

The process of dissolution of the impurity species into the alloy is governed by the diffusional characteristics of the alloy for the species like oxygen, nitrogen, and carbon. Since diffusion is a thermally activated process, it is significantly more efficient at the higher temperatures because of its exponential dependence with temperature. Thus at high temperatures, growth of the barrier layer is slowed (as seen in eq. (18)), dissolution of the barrier layer is accelerated, and the net effectiveness of the barrier layer is reduced.

High-temperature Auger electron spectroscopic studies on Ti-14Al-21Nb alloy (ref. 14) have shown that the native surface film remains stable on this alloy up to approximately 400°C, and it is completely dissolved only above about 700°C. In principle, therefore, it appears likely that the permeation results at temperatures $\leq$650°C for this alloy are a consequence of the stability of a barrier layer formed by impurities in the gas. A similar behavior has been observed for hydrogen permeation through zirconium which also shows a concurrent oxide formation and dissolution phenomenon (ref. 24).

Based on these results, the behavior of hydrogen in Ti-14Al-21Nb alloy can be classified into two major ranges based on the temperature of exposure. In the high-temperature range ($\geq$675°C), permeation of hydrogen through the alloy is controlled by the transport characteristics (diffusivity and solubility) of hydrogen in the alloy. Surface barriers, if any, are ineffective since their stability is undermined by the ability of the alloy to rapidly dissolve them. In the low-temperature range ($\leq$650°C), the permeation process is very sensitive to the surface reactions. Even small amounts of contaminants in the gas can form surface barriers that significantly lower the adsorption and dissolution of hydrogen on the

alloy surface. Further, the growth rate of barrier layers is enhanced while the dissolution kinetics are slowed down, and these layers control the permeation process.

Source of Gas Contamination

Since the hydrogen gas used in this study was procured to a specification of less than 1 ppm of impurities and was introduced into the upstream chamber after cold-trapping in liquid nitrogen, the gas supply did not appear to be the cause of contamination. The other potential cause for contamination was identified as the species desorbed from the walls of the UHV system upon backfilling with hydrogen gas. The exact nature of the phenomenon that can be described as "molecular scrubbing" is not understood, but a systematic study of this effect has been initiated in this laboratory.

Of particular relevance to the molecular scrubbing effect in the present work is the release of CO from the vacuum system in the presence of hydrogen gas. Figure 15 presents data on the mass-spectrometer peak intensities for CO and hydrogen (which relate directly to their partial pressure in the system) as a function of the total pressure of backfilled hydrogen. The peak intensities were determined using a quadrupole mass spectrometer. Observation of the ratio of CO peak intensity to hydrogen peak intensity as a function of hydrogen pressure in figure 15 indicates that the CO came from the system but not as an impurity in the hydrogen gas. For a gas impurity, this ratio should remain independent of the hydrogen pressure compared with more than an order-of-magnitude variation observed in figure 15. A further confirmation that the CO came from the system but not as an impurity in the gas was obtained from the fact that the peak intensity of CO at a constant pressure of hydrogen increased with exposure duration, whereas that of hydrogen remained constant.

The results of figure 9 can now be easily understood. At exposure temperatures $\leq$650°C with a stagnant gas, the contaminants in the gas due to molecular scrubbing were sufficient to form barrier layers that lowered the permeation rate. However, with a flowing gas stream, the permeation flux displayed the expected behavior since the contaminant species such as CO were removed fast enough from the system that dissociative adsorption of the species in the Ti-14Al-21Nb alloy was minimized.

Conclusions

Membrane permeation tests were conducted for Ti-14Al-21Nb alloy in hydrogen gas at temperatures

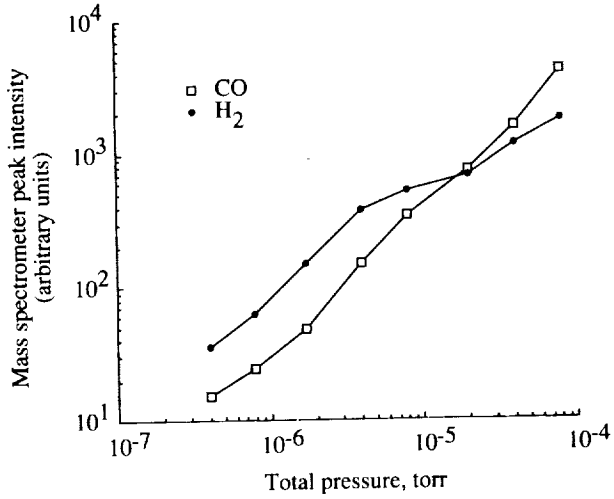

Figure 15. Variation in CO as contaminant in hydrogen gas with hydrogen pressure.

ranging from 500°C to 900°C and hydrogen pressures from 0.25 to 10 torr. Hydrogen permeability, diffusivity, and solubility were determined for the alloy. The following conclusions are drawn from the results:

1. At exposure temperatures $\geq$675°C, the permeation of hydrogen through the alloy is diffusion limited at pressures below the threshold for hydrogen-induced transformations.

2. At temperatures $\leq$650°C, permeation is limited by adsorption processes. In this range, contaminants from the walls of the permeation system dissociatively adsorb on the alloy surface and form a barrier layer (oxides and/or carbides) that inhibits the adsorption of hydrogen.

3. The stability of the barrier layer is governed by the kinetics of two competing processes: formation and dissolution. The dissolution process is dominant at temperatures $\geq$675°C so that the barrier layer does not grow in thickness and has no influence on the hydrogen permeation process.

4. The adsorbed gases on the walls of a clean ultrahigh vacuum (UHV) system are the primary source of contaminants. The adsorbed gases are released from the walls through molecular scrubbing by the hydrogen gas. Maintaining gas flow on the upstream side of the membrane removes contaminants from the system and limits their buildup in the hydrogen gas. At temperatures $\leq$650°C, where barrier-layer dissolution kinetics

are weak, the deleterious effects of molecular scrubbing can be avoided by employing gas flow.

NASA Langley Research Center
Hampton, VA 23665-5225
March 6, 1991

References

1. Shih, D. S.; Scarr, G. K.; and Wasielewski, G. E.: On Hydrogen Behavior in Ti_3 Al. *Scr. Metall.*, vol. 23, no. 6, June 1989, pp. 973–978.

2. Manor, E.; and Eliezer, D.: Hydrogen Effects in Ti_3Al-Nb Alloy. *Scr. Metall.*, vol. 23, no. 8, Aug. 1989, pp. 1313 1318.

3. McQuillan, A. D.: An Experimental and Thermodynamic Investigation of the Hydrogen-Titanium System. *Proc. of the Royal Soc. London*, ser. A, vol. 204, no. 1078, Dec. 22, 1950, pp. 309–323.

4. Lenning, G. A.; Craighead, C. M.; and Jaffee, R. I.: Constitution and Mechanical Properties of Titanium-Hydrogen Alloys. *Trans. American Inst. Min. & Metall. Eng.*, vol. 200, 1954, pp. 367–376.

5. Owen, C. V.; and Scott, T. E.: Relation Between Hydrogen Embrittlement and the Formation of Hydride in the Group V Transition Metals. *Metall. Trans.*, vol. 3, no. 7, July 1972, pp. 1715–1726.

6. Hardie, D.; and McIntyre, P.: The Low-Temperature Embrittlement of Niobium and Vanadium by Both Dissolved and Precipitated Hydrogen. *Metall. Trans.*, vol. 4, no. 5, May 1973, pp. 1247–1254.

7. Shih, D. S.; Robertson, I. M.; and Birnbaum, H. K.: Hydrogen Embrittlement of α Titanium: In Situ TEM Studies. *Acta Metall.*, vol. 36, no. 1, Jan. 1988, pp. 111–124.

8. Paton, N. E.; Spurling, R. A.; and Rhodes, C. G.: Influence of Hydrogen on Beta Phase Titanium Alloys. *Hydrogen Effects in Metals*, I. M. Bernstein and Anthony W. Thompson, eds., Metallurgical Soc. of AIME, 1981, pp. 269–279.

9. Perkins, W. G.: Permeation and Outgassing of Vacuum Materials. *J. Vac. Sci. & Technol.*, vol. 10, no. 4, July/Aug. 1973, pp. 543–556.

10. Ash, R.; Barrer, R. M.; and Palmer, D. G.: Diffusion in Multiple Laminates. *British J. Appl. Phys.*, vol. 16, no. 6, June 1965, pp. 873–884.

11. Outlaw, R. A.; Peregoy, W. K.; and Hoflund, Gar B.: *Permeation of Oxygen Through High Purity, Large Grain Silver.* NASA TP-2755, 1987.

12. Dresler, Werner; and Frohberg, Martin G. (Addis Translations International, transl.): *A Simplified Method for Determining the Coefficient of Diffusion of Hydrogen in Solid Metals.* UCRL-Trans-10651, Lawrence Livermore Lab., Univ. of California, Sept. 1972, pp. 204–209.

13. Devanathan, M. A. V.; and Stachurski, Z.: The Adsorption and Diffusion of Electrolytic Hydrogen in Palladium. *Proc. Royal Soc. London*, ser. A, vol. 270, no. 1340, Oct. 30, 1962, pp. 90 102.

14. Lee, W. S.; Sankaran, S. N.; Outlaw, R. A.; and Clark, R. K.: The Surface Variation of Ti-14Al-21Nb as a Function of Temperature Under Ultrahigh Vacuum Conditions. *J. Electrochem. Soc.*, vol. 137, no. 4, Apr. 1990, pp. 1194–1196.

15. Mueller, William M.; Blackledge, James P.; and Libowitz, George G., eds.: *Metal Hydrides.* Academic Press, Inc., 1968, pp. 69, 337.

16. Johnson, Donald L.; Shah, Kiritkumar K.; Reeves, Bruce H.; and Gadgeel, Vijay L.: *Gas Phase Hydrogen Permeation in Alpha Titanium and Carbon Steels.* NASA CR-3190, 1980.

17. Gaskey, G. R., Jr.: The Influence of a Surface Oxide Film on Hydriding of Titanium. *Hydrogen in Metals*, I. M. Bernstein and Anthony W. Thompson, eds., American Soc. for Metals, 1974, pp. 465–474.

18. Reichardt, J. W.: The Kinetics of the Hydrogen-Titanium Reaction. *J. Vac. Sci. & Technol.*, vol. 9, no. 1, Jan./Feb. 1972, pp. 548–551.

19. Wasilewski, R. J.; and Kehl, G. L.: Diffusion of Hydrogen in Titanium. *Metallurgia*, vol. 50, no. 301, Nov. 1954, pp. 225–230.

20. Shah, Kirit K.; and Johnson, Donald L.: Effect of Surface Pre-Oxidation on Hydrogen Permeation in Alpha Titanium. *Hydrogen in Metals*, I. M. Bernstein and Anthony W. Thompson, eds., American Soc. for Metals, 1974, pp. 475–481.

21. Dushman, Saul: *Scientific Foundations of Vacuum Technique*, Second ed. John Wiley & Sons, Inc., c.1962.

22. Gibb, Thomas R. P., Jr.; and Kruschwitz, Henry W., Jr.: The Titanium-Hydrogen System and Titanium Hydride. I. Low-Pressure Studies. *J. American Chem. Soc.*, vol. 72, no. 12, Dec. 1950, pp. 5365–5369.

23. Birks, N.; and Meier, G. H.: *Introduction to High Temperature Oxidation of Metals.* Edward Arnold (Publ.) Ltd. (London), 1983, p. 58.

24. Elleman, Thomas S.; Rao, Deepak; Verghese, Kuruvilla; and Zumwalt, Lloyd: *Hydrogen Diffusion, Dissolution and Permeation of Nonmetallic Solids.* ORO-4721-T1 (Contract No. DE-AS05-76ET52022), Nuclear Engineering Dep., North Carolina State Univ., [1979].

NASA
National Aeronautics and Space Administration

Report Documentation Page

1. Report No.	2. Government Accession No.	3. Recipient's Catalog No.
NASA TP-3109		

4. Title and Subtitle	5. Report Date
Surface Effects on Hydrogen Permeation Through Ti-l4Al-21Nb Alloy	April 1991
	6. Performing Organization Code
7. Author(s)	8. Performing Organization Report No.
Sankara N. Sankaran, Ronald A. Outlaw, and Ronald K. Clark	L-16826
9. Performing Organization Name and Address	10. Work Unit No.
NASA Langley Research Center Hampton, VA 23665-5225	506-43-71-01
	11. Contract or Grant No.
12. Sponsoring Agency Name and Address	13. Type of Report and Period Covered
National Aeronautics and Space Administration Washington, DC 20546-0001	Technical Paper
	14. Sponsoring Agency Code

15. Supplementary Notes

Sankara N. Sankaran: Analytical Services & Materials, Inc., Hampton, Virginia.
Ronald A. Outlaw and Ronald K. Clark: Langley Research Center, Hampton, Virginia.

16. Abstract

Hydrogen transport through Ti-14Al-21Nb (percent weight) alloy was measured using ultrahigh vacuum (UHV) permeation techniques over the temperature range from 500°C to 900°C and hydrogen pressure range from 0.25 to 10 torr. Hydrogen permeability through the alloy can be described through two different mechanisms depending on the temperature of exposure. In the range from 675°C to 900°C, the process is diffusion limited: the permeability has a weak temperature dependence, but the diffusivity has a strong temperature dependence. Below 675°C the permeation rate of hydrogen is very sensitive to surface-controlled processes such as the formation of a barrier layer from contaminants. A physical model explaining the role of surface films on the transport of hydrogen through Ti-14Al-21Nb alloy has been described.

17. Key Words (Suggested by Author(s))	18. Distribution Statement
Titanium-aluminide alloys Intermetallic alloys Hydrogen transport Hydrogen permeability Hydrogen diffusivity Hydrogen solubility	Unclassified—Unlimited Subject Category 26

19. Security Classif. (of this report)	20. Security Classif. (of this page)	21. No. of Pages	22. Price
Unclassified	Unclassified	13	A03

NASA FORM 1626 OCT 86

NASA-Langley, 1991

For sale by the National Technical Information Service, Springfield, Virginia 22161-2171